

Instrumented Indentation Test in the Nano-range: Performances Comparison of Testing Machines Calibration Methods

**Maurizio Galetto, Giacomo Maculotti,
Gianfranco Genta, Giulio Barbato &
Raffaello Levi**

Nanomanufacturing and Metrology

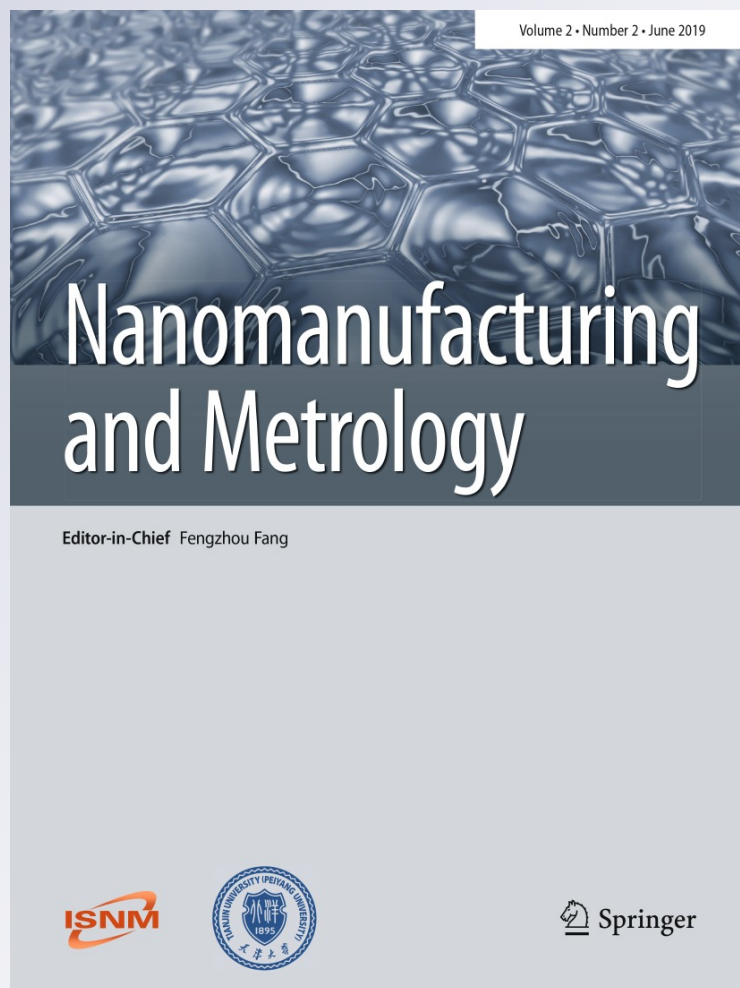
ISSN 2520-811X

Volume 2

Number 2

Nanomanuf Metrol (2019) 2:91-99

DOI 10.1007/s41871-019-00035-5



Your article is protected by copyright and all rights are held exclusively by International Society for Nanomanufacturing and Tianjin University and Springer Nature Singapore Pte Ltd.. This e-offprint is for personal use only and shall not be self-archived in electronic repositories. If you wish to self-archive your article, please use the accepted manuscript version for posting on your own website. You may further deposit the accepted manuscript version in any repository, provided it is only made publicly available 12 months after official publication or later and provided acknowledgement is given to the original source of publication and a link is inserted to the published article on Springer's website. The link must be accompanied by the following text: "The final publication is available at link.springer.com".



Instrumented Indentation Test in the Nano-range: Performances Comparison of Testing Machines Calibration Methods

Maurizio Galetto¹ · Giacomo Maculotti¹ · Gianfranco Genta¹ · Giulio Barbato¹ · Raffaello Levi¹

Received: 9 March 2018 / Revised: 2 January 2019 / Accepted: 11 January 2019 / Published online: 4 February 2019
© International Society for Nanomanufacturing and Tianjin University and Springer Nature Singapore Pte Ltd. 2019

Abstract

In the modern manufacturing industry, dealing with innovative productions and advanced materials, technological surface characterisation is becoming crucial to qualify components and optimise processes. Instrumented indentation test is an effective method for characterising mechanical behaviour of materials through the analysis of the force–displacement curve obtained during the implementation of a predefined loading/unloading cycle. Instrumented indentation test allows for hardness test to be performed at different force ranges, thus enabling bulk to local material characterisation. To guarantee the characterisation accuracy, rigorous procedures for the calibration of testing machines are defined in ISO 14577-2. In particular, calibration of frame compliance and indenter area function may be addressed according to methods which do not require the indenter area function to be known a priori, thus avoiding the need of high-resolution microscopes. The present work aims at comparing performances and compatibility of these methodologies by considering tests performed in the nano-range.

Keywords Instrumented indentation test · Frame compliance · Indenter area

1 Introduction

Instrumented indentation test (IIT) is a depth sensing technique which was introduced to assess hardness of material at nanoscales where, due to lateral resolution, traditional optical instruments are ineffective. It was early developed in the mid-1970s in the former Soviet Union [1, 2], even though, because of contingencies, it was not until the late 1980s and early 1990s; thanks to the works of Doerner and Nix [3] and Oliver and Pharr [4], it was capable to arouse actual interest in the research and industrial community.

IIT requires performing a loading–unloading cycle, throughout which applied force and indenter displacement are measured by means of devoted transducers, to indent material. With reference to Fig. 1, cycle typically consists of a loading phase, a holding at a maximum load, to compensate for creep phenomena, and an unloading. From the analysis of the loading–unloading cycle, mechanical properties can be retrieved. This mechanical characterisation requires limited sample preparation, and it can be often

considered a non-destructive test. Therefore, it is attractive for online quality control and rapid set-up of manufacturing processes. In fact, it can effectively provide throughout mechanical characterisation in terms of hardness, estimate of Young's modulus, creep and relaxation behaviour of the material [4–6]. Furthermore, it proved to be capable of characterising microstructure of metallic materials by distinguishing amongst different phases and precipitates [7] and by estimating characteristic dimension of microstructure for both mono- and polycrystalline materials [8–10]. Therefore, given the widespread appeal of this technique, it was standardised in 2002 by means of the ISO 14577, which consists of four parts, and was reissued in 2015.

Mechanical characterisation can be achieved by processing the loading–unloading cycle when expressed in terms of applied force as a function of indenter displacement, i.e. $F(h)$, the so-called indentation curve (IC), an example of which is shown in Fig. 1. However, data continuously measured during the indentation cycle require to be corrected to account for some measurement errors. In particular, h is affected by a zero error, h_0 , by the elastic deformation of the sample reference surface depending on the indenter shape, $\varepsilon F/S$ (where S is the contact stiffness, i.e. the sample stiffness, and ε caters for indenter geometry), and by the elastic deformation of the indentation testing machine, FC_f (where

✉ Maurizio Galetto
maurizio.galetto@polito.it

¹ DIGEP, Politecnico di Torino, C.so Duca degli Abruzzi 24,
10129 Turin, Italy

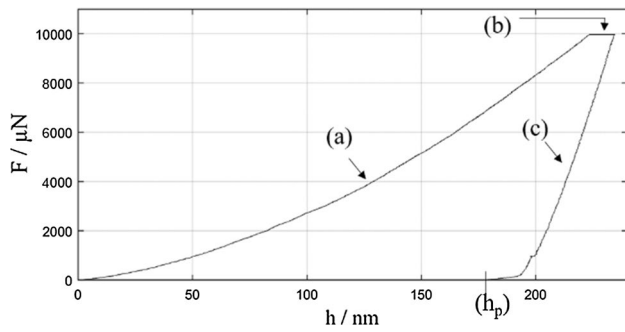


Fig. 1 Example of indentation curve: (a) loading curve, (b) holding at maximum load necessary for creep compensation, (c) unloading curve and the residual indentation h_p

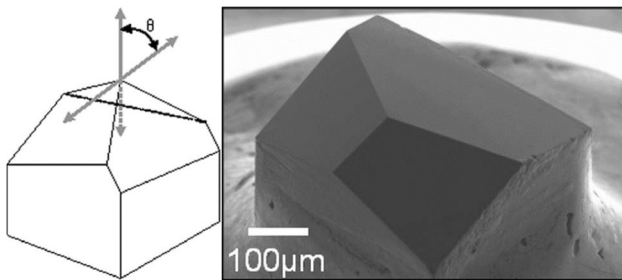


Fig. 2 Left: Berkovich indenter geometry (θ is half tip dihedral angle). Right: image of Berkovich indenter obtained with an atomic force microscope (AFM)

C_f is the frame compliance) [11]. Eventually, corrected displacement, h_c , is calculated, according to Eq. 1.

$$h_c = h - h_0 - \epsilon \frac{F}{S} - C_f F. \tag{1}$$

Furthermore, mechanical characterisation needs to estimate the contact area surface, which, being IIT a depth sensing technique, can be retrieved directly from continuous measurement of h if the area shape function, $A(h)$, is known. This relationship describes the lateral surface of the indenter as a function of the distance from its apex; for the most typical case of an ideal regular Berkovich indenter, i.e. a tetrahedron with tip dihedral angle of 130.06° (Fig. 2), it is $A(h) = 23.97h^2$. However, due to deviation from ideal geometry, which is mostly due to blunting, offset of the tip and wear, it results in a more general quadratic function, which can be written in terms of both raw (h) and corrected (h_c) displacement:

$$A(h) = a_2 h^2 + a_1 h + a_0. \tag{2}$$

When facing material characterisation, accuracy of results is core; therefore, testing machine has to be carefully calibrated according to ISO 14577-2 [12] to guarantee traceability and to establish uncertainty contribution to final results.

Recently, Barbato et al. [13] demonstrated that major contributions to measurement uncertainty of indentation modulus are the C_f and the parameters of $A(h)$. In particular, Annex D of ISO 14577-2 [12] introduces five methods for their calibration. Method nos. 1, 3 and 5 require the use of a metrological atomic force microscope (AFM) to calibrate the area shape function parameters, whilst the remaining methods (i.e. method nos. 2 and 4) outline iterative procedures to achieve calibration of both frame compliance and $A(h)$ parameters by exploiting relationships that can be drawn from IC. It is clear that adoption of metrological AFM yields lower measurement uncertainty [14]. However, considering that the availability of such a scanning force microscope (SFM) entails high cost and longer calibration time, which are critical for industrial users, often method nos. 2 and 4 are adopted. Despite this, ISO 14577-2 does not suggest a good practice to perform such calibrations and literature [14, 15] and practices of research laboratories or testing machine manufacturers show quite a variety of solution, whose compliancy is not reported.

This work aims at comparing results of C_f and parameters of $A(h)$ calibration when method nos. 2 and 4 of ISO 14577-2 are adopted. Also, it will investigate effect of different load ranges to perform calibration, in order to establish route towards good practice in calibrating testing machine. The paper is structured as follows. Section 2 describes calibration methods and experimental set-up, Sect. 3 discusses results, and Sect. 4 eventually concludes the findings.

2 Methodology

This section discusses the two methods outlined in ISO 14577-2 which will be investigated in the present work. They both rely upon some common methodology based on relationships amongst the parameters to be calibrated and on general considerations about the indentation system.

First of all, the system can be thought as a series of springs modelling the testing machine, with compliance C_f , and the sample, with stiffness S . The resulting stiffness is actually measured from raw data, according to its definition as in Eq. 3. Moreover, considering the definition of reduced modulus E_r , we can write Eq. 4, where E is Young's modulus, ν is Poisson's ratio and subscripts s and i stand, respectively, for sample and indenter. Substituting the right-hand side of Eq. 4 in Eq. 3, the linear relationship of Eq. 5 between $1/S_m$ and $1/\sqrt{A(h_{c,max})}$ is obtained, whose intercept is the C_f and from which Eq. 6 follows.

$$1/S_m = \left(\frac{\partial F}{\partial h} \Big|_{h_{max}} \right)^{-1} = C_f + 1/S \tag{3}$$

$$1/E_r = \left(\frac{1 - \nu_s^2}{E_s} + \frac{1 - \nu_i^2}{E_i} \right)^{-1} = \frac{2\sqrt{A(h_{c,max})}}{S\sqrt{\pi}} \quad (4)$$

$$1/S_m = C_{tot} = C_f + \frac{\sqrt{\pi}}{2E_r\sqrt{A(h_{c,max})}} \quad (5)$$

$$A(h_{c,max}) = \frac{\pi}{4E_r^2(C_{tot} - C_f)^2} \quad (6)$$

Thus, an iterative procedure, whose workflow is shown in Fig. 3, can be outlined to calibrate parameters and achieve convergence of the values obtained. Initialisation of the problem is performed in steps 1 and 2 assuming ideal conditions, i.e. infinitely stiff testing machine and ideal indenter geometry.

ISO 14577-2 requires a set of indentations to be performed over a load range which is representative for the application field of the instrument and suggests frame compliance initialisation to be performed exploiting data from the indentations at the two higher loads.

2.1 Method No. 2 of ISO 14577-2

Method no. 2 (M2) describes calibration to be performed according to workflow discussed in the former section by indenting a single sample. Considering that, to achieve calibration of $A(h)$ parameters, even at shallow depth, a relatively soft material is required, e.g. fused silica can be used.

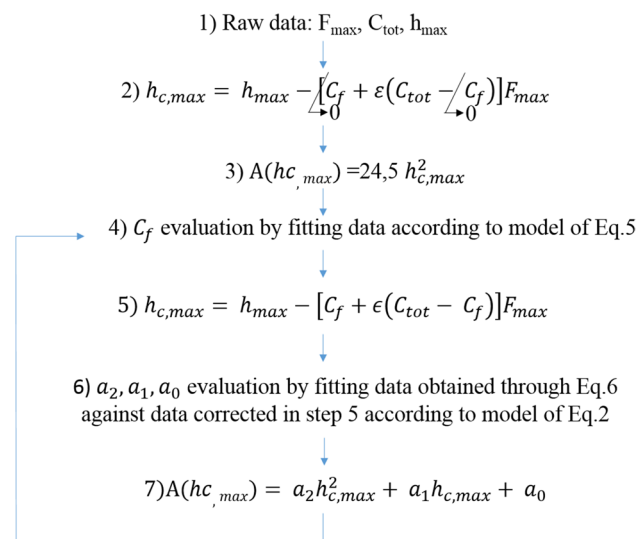


Fig. 3 Workflow of calibration iterative procedure

2.2 Method No. 4 of ISO 14577-2

Method no. 4 (M4) describes calibration to be performed according to workflow discussed in the former section by indenting two samples of different material. A stiffer material, e.g. tungsten, shall be considered to calibrate C_f , whilst a softer material, e.g. fused silica, enables the calibration of $A(h)$ parameters. Therefore, steps 1–4, and consequently 7, have to be performed considering data from tungsten indentations, whilst steps 5 and 6, which calibrate shape function parameters, require data from fused silica indentations. This method, by coupling calibration and material, guarantees faster convergence [14].

2.3 Experimental Set-Up

The present work investigates performances of calibration methods for testing equipment to perform nano-indentation. A Triboindenter TI 950 by Hysitron (shown in Fig. 4), hosted in the facilities of the Istituto Italiano di Tecnologia and equipped with a regular diamond Berkovich indenter (elastic modulus 1140 GPa and Poisson’s modulus 0.07), shown in Fig. 2, was calibrated on reference samples, whose characteristics are summarised in Table 1.



Fig. 4 Hysitron TI 950 calibrated in this work

Table 1 Calibrated material characteristics mean and expanded uncertainty

Material	Calibration laboratory	E (GPa)	ν
SiO ₂	NPL	73.3 ± 0.6	0.161 ± 0.003
W	NPL	413.0 ± 2.8	0.281 ± 0.003

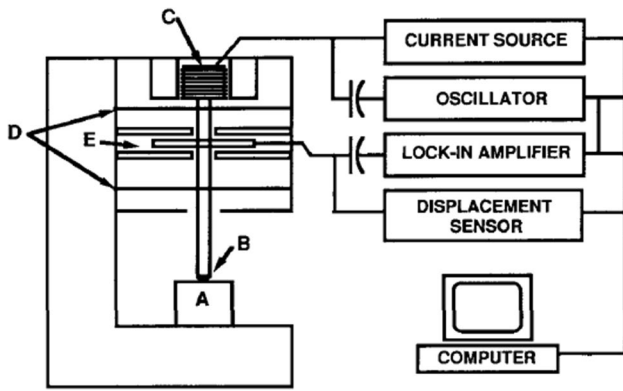


Fig. 5 A schematic representation of the testing equipment: (A) sample; (B) indenter; (C) load application coil; (D) indentation column guide springs; (E) capacitive displacement sensor [4]

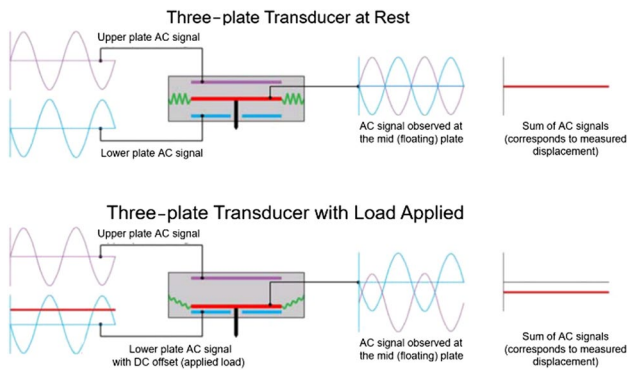


Fig. 6 Three-plate transducer actuation diagram. (Courtesy of Hysitron)

Oliver and Pharr [4] have outlined the working principle of the testing equipment and cycle, which enables the measurement of the IC. It consists of a rigid frame of which the indentation head is made up of a force and displacement transducers driven by an AC source and a controller, whose scheme is shown in Fig. 5. In particular, the TI 950 features a Hysitron-patented three-plate transducer, whose design (the scheme is shown in Fig. 6) aims at providing high sensitivity, a large dynamic range, a linear output signal and, by a low mass of the transducer mid-plate, small sensitivity to vibration. Table 2 summarises main metrological characteristics of the transducer.

Depending on the electronic circuit input, the cycle can be performed in force or displacement control. With reference to Fig. 6 and to a force-controlled cycle, the two fixed (drive) plates (violet and blue) are the electrodes that are driven by two AC voltage signals with same amplitude and a phase shift of 180°. This design makes zero the electric field potential at the mid (floating)-plate (red), which is connected to springs (green) for mechanical guide and to the output

Table 2 Metrological characteristics of three-plate force–displacement transducer

Maximum force (mN)	10
Load resolution (nN)	1
Load noise floor (nN)	100
Maximum displacement (μm)	5
Displacement resolution (nm)	0.04
Displacement noise floor (nm)	0.2

Table 3 Considered conditions for M2

Case	Material	Load range (mN)	Replications per each load
M2_1	SiO ₂	0.5–1–5–10	10 ×
M2_1_bis		0.5–1–5–10	5 ×
M2_1_ter		0.5:0.25:10	1 ×

Table 4 Considered conditions for M4

Case	Material	Load range (mN)	Replications per each load
M4_1	W	0.5–1–5–10	10 ×
M4_1_bis	SiO ₂	0.5–1–5–10	5 ×
M4_1_ter	W	0.5:0.25:10	1 ×
	SiO ₂		

electrode. Force is applied electrostatically by means of a DC voltage bias at the lower plate. The three-plate design generates a linear electric field voltage, and because the input impedance is significantly larger than the output's, the floating electrode electric potential is the same of the electric field at its location. Thus, by continuously recording the input voltages, e.g. both the AC and the DC, at the drive plates and the resulting output voltage at the floating plate, its resulting displacement can be retrieved by the known, by design, electric field.

2.4 Experimental Plan

The present work investigates the effect of method and load, in terms of steps within a given range, on the results of calibration of frame compliance and area shape function parameters as average values and related uncertainties.

According to the literature [12, 14, 15], the experimental plan, summarised in Tables 3 and 4, was outlined to properly cater for different degrees of freedom. The full force range of the commercial indentation platform Hysitron TI 950, i.e. from 0.5 to 10 mN, was considered. To cater for replicated

measurements effect, the range was sampled according to a logarithmic scale; at these levels, ten and five replicated measurements were performed (respectively case “1” and “1_bis”). Furthermore, the force range was sampled at 0.25 mN, as trade-off between data set size and measurement time (case “1_ter”), to investigate effect of high-density individual measurements. Calibrated samples made out of fused silica and tungsten, due to their homogeneity and difference in mechanical properties (as reported in Table 1), were selected as calibration materials.

The measured contact stiffness is evaluated according to the power law method, described in ISO 14577-1 [6]. Sneddon’s general solution of Boussinesq’s problem states that the unloading curve (Fig. 1) yields a power law (PL) relationship between force and displacement, as shown by Eq. 7, in which the exponent m depends on the indenter geometry (for Berkovich indenter theoretical value is $m = 2$), whose equation can be obtained by fitting the experimental raw data. This analytical model is then differentiated to obtain S_m according to its definition in Eq. 3.

$$F = \alpha h^m. \tag{7}$$

Custom script was implemented on *MATLAB R2018b*, convergence was achieved as soon as the variation of mean values of calibrated parameter between cycle j and $j - 1$ was less than 0.1%, and it was furtherly checked on root-mean-square error stabilisation. To bound least-squared linear regression to the physics of the problem, additional constraints were set to force the intercept of the linear model (step 4 in Fig. 3) and the evaluated contact area (step 7 in Fig. 3) to be positive.

Uncertainty evaluation of the four calibrated parameters (a_0 , a_1 , a_2 and C_f) is addressed to cater for the several influencing factors, i.e. calibrated sample and indenter material properties uncertainty, testing equipment force and displacement transducers accuracy and the regressions within the iterative procedure itself. Ishikawa diagram in Fig. 7 summarises influencing factors.

Individual contributions, which are represented by influencing factors covariances, can be combined according to Eq. 8 [16]: f is a generic function of the inputs x , i.e. the influencing factors, and $u(x_i, x_j)$ is the covariance associated with x_i and x_j ;

partial derivatives are the sensitivity coefficients, which cater for sensitivity of the output y on the inputs x .

$$u_c^2 = \sum_{i=1}^N \sum_{j=1}^N \frac{\partial f}{\partial x_i} \frac{\partial f}{\partial x_j} u(x_i, x_j). \tag{8}$$

Combined uncertainty, u_c , is calculated, and when multiplied by a coverage factor k , the expanded uncertainty, U , which is half width of the confidence interval, is evaluated. k depends on the confidence level at which U is computed and on the probability distribution of y ; typically, $k = 2$ corresponds to a confidence level of about 95% [16]. However, iterative computation hinders from writing explicit and independent relationships for the four calibrated parameters, which are necessary to apply Eq. 8. Therefore, according to JCGM 100 (GUM) [16] and to JCGM 101 [17], a Monte Carlo simulation was set up to provide an assessment of the expanded uncertainty, with a confidence level of 95%, of the calibrated parameters.

3 Results and Discussion

This section discusses calibration results obtained by applying the standard methods M2 and M4 to the cases listed in Tables 3 and 4.

Results are discussed in terms of relative consistency amongst the methods, expanded uncertainty, method computational speed and correctness of the estimation. In particular, the method speed is evaluated in terms of iteration to achieve convergence, as this impacts on the calibration cost and computational effort. Estimate correctness is addressed for C_f and a_2 and a_0 . The first parameter is expected, from experience, to have order of magnitude at most of $10^{-3} \text{ mm}\cdot\text{N}^{-1}$; the second, due to deviation from ideal geometry, is expected to be in the neighbourhood of its theoretical value, i.e. 23.97; the third, provided that the indenter mounted on the machine was not brand new, should cater for the faster increase in contact area at small penetration depths, and hence it is expected to be slightly positive [6, 11–15]. Even though wear and tip blunting affect the whole area shape function, so that a_0 , a_1 and a_2 deviations from theoretical values are intertwined, simple forecast can be only made for a_0 and a_2 .

Figures 8, 9, 10 and 11 show results for the calibrated parameters, respectively, a_0 , a_1 , a_2 and C_f . Error bars of the figures represent expanded uncertainty with coverage factor equal to 2: black error bars graph overall variability, whilst green bars the variability component due to regression.

The different methods show that the mean estimate of a_2 and C_f quite oscillates about the expected value, which in some cases may result in bias, e.g. M2_1 and M2_1_bis provide relatively underestimated means. This notwithstanding, they all, but for the couple M2_1 and M4_1, provide results compatible with each other, even though this is

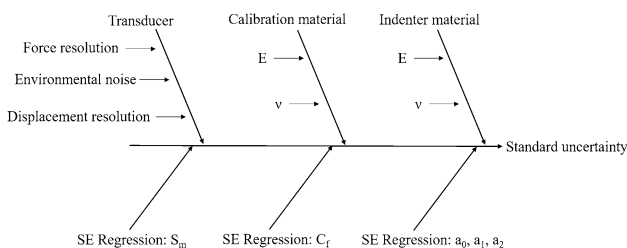


Fig. 7 Ishikawa diagram for influencing factors of standard uncertainty. SE stands for standard error

Fig. 8 Comparison of calibration methods. Parameter a_0 . Error bars represent expanded uncertainty with coverage factor 2: black—overall variability, green—regression variability

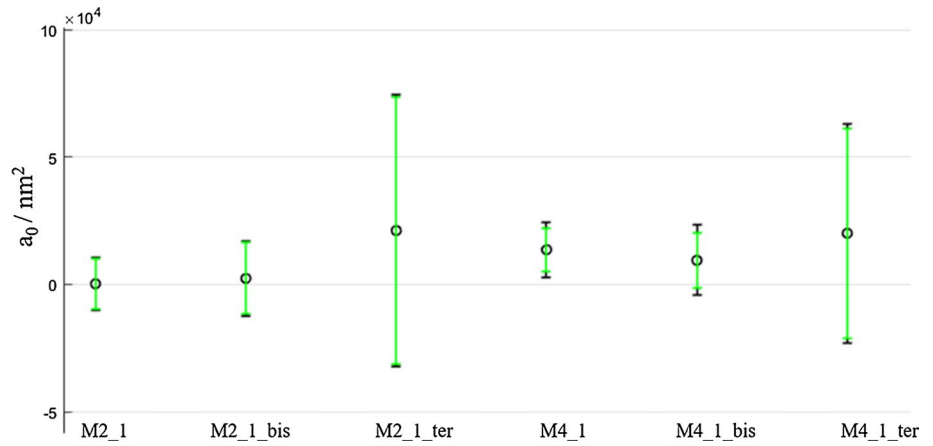


Fig. 9 Comparison of calibration methods. Parameter a_1 . Error bars represent expanded uncertainty with coverage factor 2: black—overall variability, green—regression variability

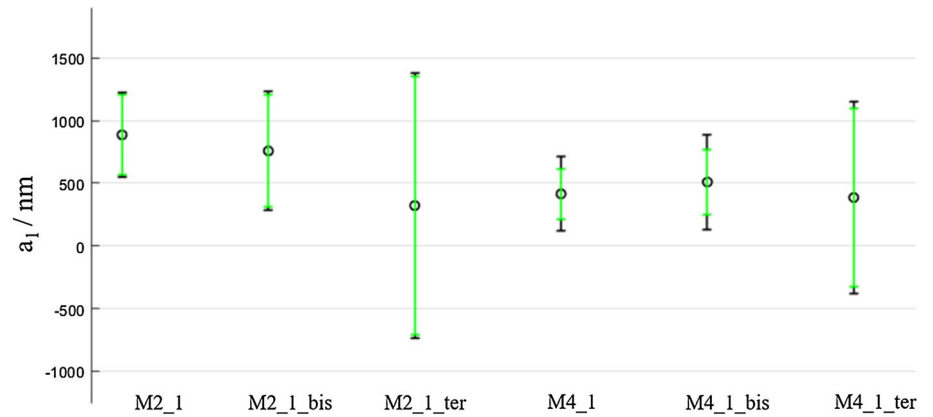
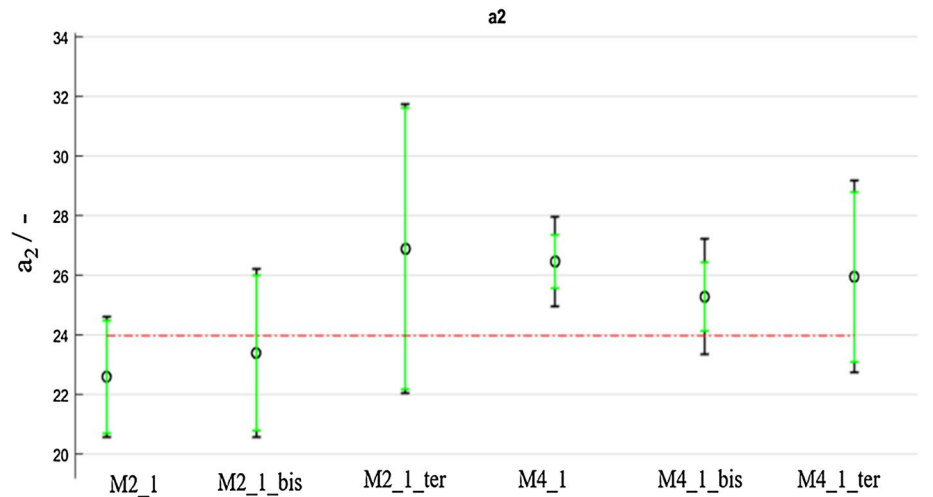


Fig. 10 Comparison of calibration methods. Parameter a_2 . Error bars represent expanded uncertainty with coverage factor 2: black—overall variability, green—regression variability. Red dash-dotted line is theoretical value



mostly thanks to the high expanded uncertainty, as shown in Table 5, which summarises relative expanded uncertainties at a confidence level of 95%. For reference, average estimates of parameters are reported in Table 6.

As expected, cases with five load replications provided higher uncertainty to the measurement than ten replication cases. Even greater variability occurs when continuously

increasing loads are adopted in the calibration procedure, though they should provide higher data density improving the fitting. In fact, when continuously increasing loads are adopted, Monte Carlo simulation shows the larger variability associated with the method definition since extracting single values from several distributions yields larger uncertainty than extracting multiple values from a smaller number of distributions.

Fig. 11 Comparison of calibration methods. Parameter C_f . Error bars represent expanded uncertainty with coverage factor 2: black—overall variability, green—regression variability

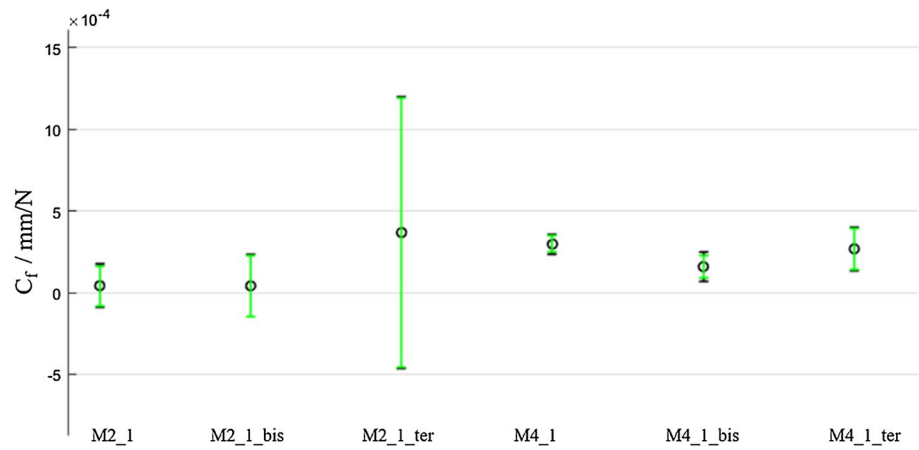


Table 5 Relative expanded uncertainties (at a confidence level of 95%) of calibrated parameters

Method	$U_{rel C_f} (%)$	$U_{rel a_0} (%)$	$U_{rel a_1} (%)$	$U_{rel a_2} (%)$
M2_1	> 100	> 100	38	9
M2_1_bis	> 100	> 100	62	12
M2_1_ter	> 100	> 100	> 100	18
M4_1	20	78	71	6
M4_1_bis	55	> 100	74	8
M4_1_ter	51	> 100	> 100	12

Table 6 Average value of calibrated parameters

Method	$C_f (\mu\text{m}\cdot\text{N}^{-1})$	$a_0 (\text{nm}^2)$	$a_1 (\text{nm})$	a_2
M2_1	0.043	226	886	22.59
M2_1_bis	0.041	2336	758	23.38
M2_1_ter	0.368	21,124	322	26.87
M4_1	0.297	13,597	415	26.45
M4_1_bis	0.159	9434	510	25.27
M4_1_ter	0.268	20,054	386	25.95

C_f is expected to be at most $1 \mu\text{m}\cdot\text{N}^{-1}$, a_0 to be positive and a_2 about 23.97

In general, the use of two materials, i.e. method no. 4, yields lower uncertainty, thanks to the slight decoupling of frame compliance and area shape function parameters evaluation that is achieved by means of this procedure; in particular, method no. 2 is associated with poor performances generating relative uncertainties larger than 100%, which makes this method questionable for metrological purposes. However, high relative uncertainties are always expected when dealing with small numbers, i.e. mainly in the case of a_0 . Furthermore, regression variability is the main uncertainty contribution and M4_1 produces the smallest expanded uncertainties.

Consistently with Herrmann et al.'s [14] results, M4 provides faster convergence with less than ten iterations for all the cases, whilst M2 requires, depending on the case, about thirty iterations for M2_1 and M2_1_bis and sixty for M2_1_ter.

Parameters are correctly estimated with respect to their theoretical value in all the cases, though high expanded uncertainty deeply affects these results; however, M4_1 represents an exception in this case as will be discussed in the following. As far as a_2 is concerned, M2_1 and M2_1_bis tend to relatively underestimate the mean value.

Area shape function parameter a_0 results to be slightly positive, as expected, and to include the nominal zero value in all the cases but for M4_1. Frame compliance calibration shows that a small but non-negligible correction is required to cater properly for testing equipment stiffness.

To conclude, C_f and a_2 calibration provides an interesting validation of the results: provided the relationship established between these two parameters in Eq. 5, a proportionality is expected between their mean estimates, which is in fact shown comparing Figs. 10 and 11.

4 Conclusions

The present work discussed iterative methods for calibrating area shape function parameters and frame compliance for instrumented indentation testing equipment. These parameters were demonstrated to be major source of uncertainty in mechanical characterisation by means of instrumented indentation test, and the calibration methods considered are broadly adopted in practice because they do not require scanning force microscopes. Calibration methods are described in the related standard ISO 14577-2, and the present work investigates some degrees of freedom of the calibration procedure in the nano-range, which have been defined according to laboratories practice and literature references of the standards.

Methods show high expanded uncertainty resulting in poor precision which disguises a general lack of robustness and is enhanced when only one material for calibration is adopted, i.e. method no. 2. Method no. 4 yields more precise results with less computational effort, thanks to the different materials adopted for the calibration of the frame compliance and area shape function parameters. Even if method M4_1 is the most precise, its accuracy might be questioned.

Monte Carlo simulation showed that regression generates the larger contribution to uncertainty. Moreover, uncertainty is strongly dependent on the data set size and, in particular, it benefits from replicated data.

The standard appears to be little prescriptive since expanded uncertainty and accuracy of the results significantly depend on the choice of the method and its implementation. The authors highlight that further analysis shall be conducted to improve traceability of the instrumented indentation test, and they are working in that direction.

Acknowledgements The authors would like to thank Dr Massimo Lorusso of Istituto Italiano di Tecnologia for his availability and expertise in operating the testing equipment and for having performed the measurements.

References

- Alekhin VP, Berlin GS, Shorshorov MC (1971) Instruments for micromechanical tests of solid materials. *Instrum Exp Tech USSR* 14(4):1265
- Lucca DA, Herrmann K, Klopstein MJ (2010) Nanoindentation: measuring methods and applications. *CIRP Ann Manuf Technol* 59(2):803–819
- Doerner MF, Nix WD (1986) A method for interpreting the data from depth-sensing indentation instruments. *J Mater Res* 1: 601–609
- Oliver WC, Pharr GM (1992) An improved technique for determining hardness and elastic modulus using load and displacement sensing indentation experiments. *J Mater Res* 7(6):1564–1583
- Oliver WC, Pharr GM (2004) Measurement of hardness and elastic modulus by instrumented indentation: advances in understanding and refinements to methodology. *J Mater Res* 19(1):3–20
- ISO 14577-1:2015 Metallic materials-instrumented indentation test for hardness and materials parameters-part 1: test method. ISO, Genève, Switzerland
- Engqvist H, Wiklund U (2004) Mapping of mechanical properties of WC-Co using nanoindentation. *Tribol Lett* 8(2–3):147–152
- Nix WD, Gao H (1998) Indentation size effect in crystalline materials: a law for strain gradient plasticity. *J Mech Phys Solids* 46(3):411–425
- Kim JY, Kang SK, Lee JJ, Jang J, Lee YH, Kwon D (2007) Influence of surface-roughness on indentation size effect. *Acta Mater* 55(10):3555–3562
- Hou X, Jennett NM, Parlinska-Wojtan M (2013) Exploiting interactions between structure size and indentation size effects to determine the characteristic dimension of nano-structured materials by indentation. *J Phys D Appl Phys* 46(26):265301
- Cagliero R, Barbato G, Maizza G, Genta G (2015) Measurement of elastic modulus by instrumented indentation in the macro-range: uncertainty evaluation. *Int J Mech Sci* 101–102:161–169
- ISO 14577-2:2015 Metallic materials-instrumented indentation test for hardness and materials parameters-part 2: verification and calibration of testing machines. ISO, Genève, Switzerland
- Barbato G, Genta G, Cagliero R, Galetto M, Hlopstein MJ, Lucca DA, Levi R (2017) Uncertainty evaluation of indentation modulus in the nano-range: contact stiffness contribution. *CIRP Ann Manuf Technol* 66:495–498
- Herrmann K, Jennett NM, Wegener W, Meneve J, Hasche K, Seeman R (2000) Progress in determination of the area function of indenters used for nanoindentation. *Thin Solid Films* 377–378:394–400
- Meneve JL, Smith JF, Jennett NM, Saunders SRJ (1996) Surface mechanical property testing by depth sensing indentation. *Appl Surf Sci* 100–101:64–68
- JCGM 100:2008, Evaluation of measurement data—guide to the expression of uncertainty in measurements (GUM), JCGM, Sèvres, France
- JCGM 101:2008, Evaluation of measurement data—supplement 1 to the “Guide to the expression of uncertainty in measurement”—propagation of distributions using a Monte Carlo method, JCGM, Sèvres, France



Maurizio Galetto received the Master of Science Degree in Physics from University of Turin, Italy, in 1995 and the PhD Degree in “Metrology: Measuring Science and Technique” from Politecnico di Torino, Italy, in 2000. He is currently Full Professor at the Department of Management and Production Engineering (DIGEP) of the Politecnico di Torino, where he teaches “Quality Engineering” and “Experimental Statistics and Mechanical Measurement”. He is Associate Member of CIRP

(The International Academy for Production Engineering) and Fellow of A.I.Te.M. (Associazione Italiana di Tecnologia Meccanica) and E.N.B.I.S. (European Network for Business and Industrial Statistics). He is Member of the Editorial Board of the scientific international journal *Nanomanufacturing and Metrology* and collaborates as referee for many international journals in the field of Industrial Engineering. He is author and coauthor of 4 books and more than 100 published papers in scientific journals, and international conference proceedings. His current research interests are in the areas of Quality Engineering, Statistical Process Control, Industrial Metrology and Production Systems. At present, he collaborates in some important research projects for public and private organizations.



Giacomo Maculotti received the Master of Science Degree in Automotive Engineering in 2017 from Politecnico di Torino, Italy. He is currently PhD student at Politecnico di Torino - Dept. of Management and Production Engineering (DIGEP). His current research interests are Industrial Metrology, Technological Surfaces Characterization, and Quality Engineering.



Gianfranco Genta received the Master of Science Degree in Mathematical Engineering from Politecnico di Torino, Italy, in 2005 and the PhD Degree in “Metrology: Measuring Science and Technique” from Politecnico di Torino in 2010. He is currently Fixed-Term Researcher at the Department of Management and Production Engineering (DIGEP) of the Politecnico di Torino, where he has been teaching “Experimental Statistics and Mechanical Measurement” since 2012. He is Research Affiliate of

CIRP (The International Academy for Production Engineering) and Fellow of A.I.Te.M. (Associazione Italiana di Tecnologia Meccanica). He is author and coauthor of 3 books and more than 40 publications on national/international journals and conference proceedings. His current research focuses on Industrial Metrology, Quality Engineering and Experimental Data Analysis.



Giulio Barbato received the Master of Science Degree in Nuclear Engineering in 1971, and subsequently the Degree in Aeronautical Engineering from Politecnico di Torino, Italy. He started his career in 1972 at IMGC (Istituto di Metrologia “Gustavo Colonnetti”), where he worked in the fields of Stress Analysis, Force Measurement and Hardness Measurement. In 1973 he started his cooperation with Politecnico di Torino as teaching assistant in “General Metrology”. In 1994 he received the

chair of Full Professor of “Mechanical Measurement”. In 1997, he was called to the chair of “General Metrology” at the Politecnico di Torino. He retired in 2017 and currently he teaches “Experimental Statistics” and “Mechanical Measurement” at the Politecnico di Torino as Contract Professor.



Raffaello Levi received the Master of Science Degree in Industrial Engineering in 1959 from the Politecnico di Torino, Italy. He is Emeritus Professor at the Department of Management and Production Engineering (DIGEP) at the Politecnico di Torino. He was the chair of “Manufacturing Technology” and “Machine Construction and Drawing” at the Politecnico di Torino from 1972 to 2010. Currently he teaches “Design of Industrial Experiments” for PhD courses at the Politecnico di

Torino as Contract Professor. He is Honorary Fellow of CIRP (The International Academy for Production Engineering). His research interests are in the areas of Experimental Mechanics, Industrial Metrology, Manufacturing Technology, Applied Statistics and Design of Experiments.